Multi-material direct ink writing (DIW) for complex 3D metallic structures with removable supports

*Chao Xu, Bronagh Quinn, Gilles L'Espérance, Louis Laberge Lebel, Daniel Therriault**

Chao Xu, Bronagh Quinn, Prof. Louis Laberge Lebel, Prof. Daniel Therriault
Mechanical engineering, Polytechnique Montreal
C.P. 6079, succ. Centre-Ville, Montreal, QC H3C 3A7, Canada
E-mail: Daniel.therriault@polymtl.ca
Prof. L'Espérance
Metallurgy engineering, Polytechnique Montreal
C.P. 6079, succ. Centre-Ville, Montreal, QC H3C 3A7, Canada

Keywords: additive manufacturing, direct ink writing, complex 3D metallic structures, removable support, multi-material

Abstract

Direct ink writing (DIW) combined to post-deposition thermal treatments is a safe, cheap and accessible additive manufacturing (AM) method for the creation of metallic structures. Single material DIW enables the creation of complex metallic 3D structures featuring overhangs, lengthy bridges or enclosed hollows, but requires the printing supporting structures. However, the support printed from the same material becomes inseparable from the building structure after the thermal treatment. Here, a multi-material DIW method is developed to fabricate complex three-dimensional (3D) steel structures by creating a removable support printed from a lower melting temperature metal (i.e., copper) or a ceramic (i.e., alumina). The lower melting temperature metal completely infiltrates the porous steel structures for a hybrid configuration, while the ceramic offers a brittle support that can be easily removed. The influence of the support materials on the steel structure properties is investigated by the characterizing the dimensional shrinkage, surface roughness, filament porosity, electrical conductivity and tensile properties. The hybrid configuration (i.e., copper infiltrated steel structures) improves the electrical conductivity of the fabricated steel structure by 400% and the mechanical stiffness by

34%. The alumina support is physically and chemically stable during the thermal treatment, bringing no significant contamination to the steel structure.

Introduction

Metallic structures fabricated through Additive manufacturing (AM), also referred to as three-dimensional (3D) printing, have been used as batteries,[1-2] medical implants,[3-4] and sensors[5-6] due to their key advantages, i.e., high mechanical and electrical properties, complex geometries, and mold-free manufacturing processes. The most established metal AM approaches are powder-bed based methods such as selective laser melting (SLM) and electron beam melting (EBM).[7-9] They use a laser beam or electron beam to locally fuse metallic particles in a powder bed to build a 3D object layer-by-layer. These methods feature short manufacturing time, high mechanical performance of the fabricated parts and very few restrictions on the printed geometry. However, they are limited by high cost, laser induced excessive oxidation, and residual stresses in the fabricated parts.[10-12]

Researchers developed many different metal AM methods to overcome the shortcomings of the powder-bed methods. Skylar-Scott *et al.* built metallic architectures from a water-based silver ink. The silver ink was extruded from a micro nozzle as a filament. The filament was sintered right after extrusion using a laser beam.[13] Freeform 3D metallic architectures featuring high resolution and high electrical conductivity were fabricated using this method. However, the laser beam sintering in the air would cause excessive oxidation and loss of alloying elements. Wang *et al.* developed an initiator-integrated 3D printing method to build metallic structures.[14] First, a polymer template of the 3D structure was built. Then metallic particles were deposited on the surface of the polymer template through electroless plating. Finally, the polymer template was etched away to achieve ultralight cellular metallic structures. This method enables the fabrication of complex 3D metallic structures featuring low density. However, the metallic architecture is hollow and relatively thin after the polymer template is etched away, which leads to poor mechanical performances.

Direct ink writing (DIW) is an AM method, which usually relies on the extrusion of polymer solution (or melt), known as ink, through a micro-nozzle and the deposition of the extruded ink on a substrate layer by layer to create a 3D object.[15-16] Researchers adapted it to metal AM by printing from metallic inks.[17-20] The metallic inks are prepared by adding metal micro- or nano-particles to the polymer solution (or melt), which are used in DIW to build a metal-polymer composite 3D structure. To achieve a metallic structure featuring high mechanical and electrical performances, a post-deposition thermal treatment is performed to pyrolyze the polymer and to sinter the metal particles.

DIW of polymer can create complex 3D structures with large overhangs or lengthy bridges by printing support underneath them to hold the structures. Once the printing is completed, the sacrificial support is removed.[21-22] However, the utilization of a support does not work for DIW of metal, where a post-deposition thermal treatment is performed. If the support is removed before the thermal treatment at a moment when the polymer binder is pyrolyzed before the sintering of the metallic particles, the overhang features will collapse. Whereas, if the support printed from the same material is not removed before the thermal treatment, the support and the building structure will fuse together and become inseparable after the thermal treatment. Thus, the existed DIW methods are unable to fabricated complex 3D metallic structures featuring overhangs, length bridges or enclosed hollows.

Here, we propose a multi-material DIW method to fabricate complex 3D metallic structures with removable supports. This method consists of two steps: (a) room-temperature DIW of metal-polymer composite structures with metal- (or ceramic-) polymer composites supports, and (b) a post-deposition thermal treatment turning the as-printed metal-polymer composite structures to metal structures. **Figure 1a** shows a schematic of the multi-material DIW system and as-printed hollow sphere structures. The multi-material DIW system includes three major components: (i) a computer controlled 3-axis robot, (ii) a pressure dispenser, and (iii) multiple ink syringes containing steel, copper and alumina inks. The inks are concentrated steel, copper and alumina microparticle suspensions dispersed in a polymer solution (i.e., polylactic acid / dichloromethane, referred to as PLA/DCM), respectively. The scanning electron microscope (SEM) images of the microparticles are shown in **Figure S1**. To fabricate a 3D metallic structure, e.g., a hollow sphere as shown in **Figure 1a**, supports are generated inside the hollow sphere to support the top overhang part and underneath the sphere to create a flat bottom which is compatible with the geometry of the substrate. Here, as a proof of concept, the supports are built using a secondary material (i.e., copper or alumina ink), while the building structure is printed with the primary material (i.e., steel ink). The steel-PLA composite structure with copper-PLA composite support is referred to as as-printed S-Cu, while the one with alumina-PLA composite support is referred to as as-printed S-Al_2O_3. These two types of supports are differently removed through the post-deposition thermal treatment. The lower melting temperature metallic support (i.e., copper) could be completely melted and infiltrated into the pores within the filament of the sintered structure to achieve a hybrid configuration. The ceramic support (i.e., ceramic) survives the temperature cycle without any significant sintering and can be easily removed without affecting the metallic structure.

Figure 1b presents the temperature profile of the thermal treatment, the thermal gravity analysis (TGA) result of the polymer binder PLA under this temperature profile, the sintering temperature range and melting temperature of stainless steel 316L and copper.[23-24] In addition, a schematic is shown in **Figure 1b** illustrating the microstructure variations of the two-phase interface in the as-printed structures at five different stages during the thermal treatment. For S-Cu structures, Stage I is an as-printed structure at room temperature, where the steel and copper particles are bound by the PLA binder, respectively. Stage II consists of a one-hour plateau at 400°C for debinding. PLA binder is completely pyrolyzed as shown in the TGA curve, where the weight of the PLA binder rapidly drops within 7 min. The structure is held by the friction forces among the steel particles and among copper particles, respectively. The temperature then is increased to reach a temperature plateau at 950°C for one hour (Stage III). This plateau temperature is selected to be in the sintering temperature range of S316L and copper, but is lower than their melting temperatures. The S-Cu structure is mechanically enhanced by initial sintering, where the necks appear among steel particles and among copper particles, respectively. After this stage, even if the support is removed, the bonding between the steel particles is strong enough to hold the building structure. During Stage IV, the temperature increases from 950°C to 1165°C, surpassing the melting temperature of copper (i.e. 1085°C). The copper support starts melting, while the steel structure is held in its original geometry by the sintering bonds generated during Stage III. Stage V is a four-hour plateau at 1165°C, where the steel particles are further sintered and the melted copper completely infiltrates the pores of the sintered steel structure by capillary forces. After this temperature profile, the as-printed S-Cu is turned into a steel structure infiltrated by the copper.

For S-Al_2O_3 structures, Stages I and II are the as-printed structure at room temperature and the debinding process respectively, like those of the S-Cu structures. Since both the melting temperature of alumina (2040°C) and the lower limit of alumina sintering temperature (1800°C)[25] are much higher than the maximum imposed temperature (1165°C), the alumina particles are neither melted nor sintered, but remain as individual particles during the whole thermal treatment. Therefore, in Stages III to V, the alumina support preserves its shape mostly due to the friction forces among the alumina particles. The steel particles are sintered and form a strong steel keeping the original geometry. As the alumina support is weakly held by the friction forces, it does not fuse with the building structure and can be easily removed by hand after the thermal treatment.

Figure 1c shows the as-printed and sintered S-Cu and S-Al_2O_3 printed using this method as a structure shaped as a human thigh bones at a scale of 1:7. The steel bone structure is 50% of volume filled, while the support structure is 30% of volume filled. The supports provide a flat bottom and hold up the overhang features for the bone to facilitate the printing on a flat substrate. After the thermal treatment, the copper support melts and infiltrates into the sintered steel structure, while the alumina support is removed easily by hand. Both sintered structures preserve the original geometry of the human thigh bone with a uniform linear dimensional shrinkage of 11%. To demonstrate the ability to build complex 3D metallic structure featuring overhangs, an inverted "L" shape structure featuring a large overhang part is fabricated through this method with a cubic support structure printed from a secondary material (**Figure S2**).

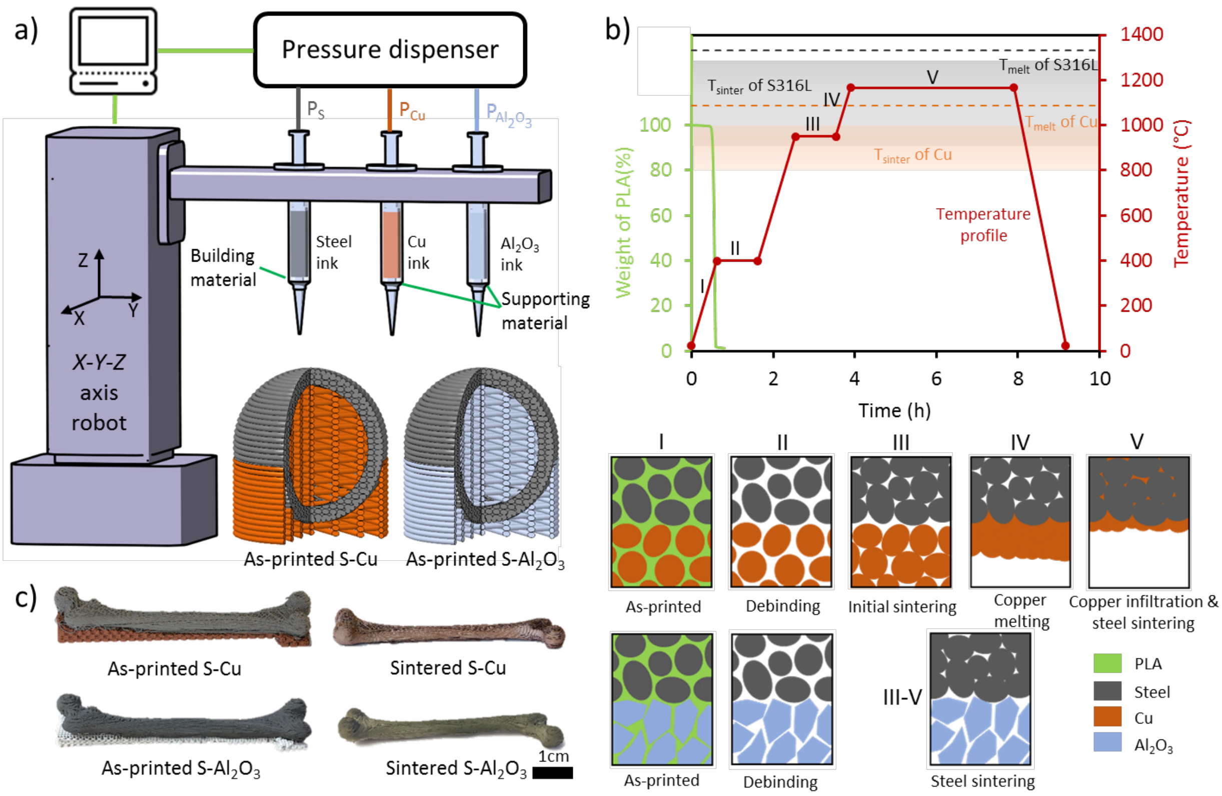

Figure 1. Multi-material DIW for complex 3D metallic structures with removable supports consists of two steps: (a) room-temperature DIW of metal-polymer composite structures with metal- (or ceramic-) polymer composites supports, and (b) a post-deposition thermal treatment turning the as-printed metal-polymer composites structures to metal structures, and a schematic shows the two-phase interface microstructures variations of the as-printed structures at five

different stages during the thermal treatment. (c) Optical images of as-printed and sintered S-Cu and S-Al_2O_3 structures printed as a human thigh bones at a scale of 1:7.

Experimental Section

Ink preparation: The steel particles are stainless steel 316L with a spherical shape and a diameter less than 20μm. The copper particles are spherical and less than 20μm in diameter. The steel and copper particles are purchased from US Research Nanomaterials, Inc. The alumina particles are irregular in shape and less than 10μm in size (265497, Sigma-Aldrich). The SEM images of the three types of particles are presented in **Figure S1**. The polymer binder solution is produced by adding 2g polylactic acid (PLA, 4032D, Natureworks LLC) to 8g dichloromethane (DCM, Sigma-Aldrich) and left to dissolve for 24 h to ensure homogenization. The steel, copper and alumina inks are prepared by mixing the corresponding particles with the polymer solution at a weight ratio of 3:1, 3:1, and 1.2:1, respectively, using a ball mill mixer (8000M Mixer/Mill, SPEX SamplePrep) for 15 min.

Multi-material DIW: The CAD model of the building structure is either designed in a computer aided design software (CATIA) or downloaded from internet (thingerverse.com). The support is generated where it is needed to hold building structure through a software, Simplify 3D (version 4.0). Both the building and support structures are converted into a G-code using Simplify 3D. Then the G-code is converted into a point-to-point program that can be read by the JR Point software to control the 3-axis positioning robot (I&J2200-4, I&J Fisnar). The ink is loaded in a syringe (3mL, Nordson EFD) attached with a smooth-flow tapered nozzle (exit inner diameter = 250μm, Nordson EFD). DIW is performed using the positioning robot and pressure dispensing systems (HP-7X, Nordson EFD). The structures are deposited on a glass slide (PN 16004-422, VWR) at room temperature. All the structures in this work are deposited at a linear printing speed of 15mm/s and under an applied pressure of 0.7 - 1.2 MPa. The spacing between each layer is 80% of the nozzle inner diameter to compensate the solvent evaporation induced filament shrinkage and ensure tight bonding between the adjacent layers.

Post-deposition thermal treatment: The as-printed structures are thermal treated in a laboratory electric tubular furnace (59256-P-COM, Lindberg) on a ceramic substrate. To prevent oxidation, a gas flow (97.5% Ar and 2.5% H_2, flow rate = 5 L/min) is circulated inside the quartz tube. The temperature profile is presented in **Figure 1b**, wherein all the heating rates are 600°C/h and the cooling rate is 900°C/h.

Surface roughness measurement: The roughness of the top surface of the sintered steel structures is measured using a profilometer (SV-C4000, Mitutoyo) following the AISI standard in accordance with ASME B.46.1-2002. The measuring direction is perpendicular to the filament orientation. The sampling length of meso R_a is 7.5mm, while the sampling length of micro R_a is 0.1mm. Ten specimens are measured for each sample type.

Porosity analysis: The sintered steel scaffold is cut parallel to the *Z* direction to observe the vertical cross section. The sliced steel scaffold is sealed in a resin (EpoFix resin, Struers) block and the cross section is polished for observation under an optical microscope (Zeiss Axioplan EL-Einsatz). The porosity is determined using an image analysis software (ImageJ). The filament porosity is calculated as the ratio of void area inside the filament over the filament area. Ten cross sections of each sample are analyzed.

Electrical conductivity analysis: The electrical conductivity of the sintered steel structures is measured using the four-point probes method. A constant current of 1A is provided by a power supply (Agilent, E3633A). The voltage is acquired by a multimeter (HP, 3457A). Five specimens of each sample type are tested.

Tensile test and DIC: The samples are sintered steel tensile bars, of which the cross-section of the neck is ~3.6 × 1.8 mm. The tensile tests are carried out in a MTS Insight machine with a 50 kN load cell (MTS 569332-01) at a crosshead speed of 1 mm/min and using DIC to measure the strain of the tensile bars. The tensile bars are polished on both sides for a smooth surface. A thin layer of white acrylic spray paint (Ultra 2X spray paint, Painter's Touch) is applied on the surface. The speckle pattern (black dots of ~0.4mm) is painted on the white paint with a roller brush to ensure the tracking of displacement. The images of the sample are taken by two long range focus stereo microscopes at a frequency of 4Hz during the tensile test. The images are analyzed by VIC3D micro (Correlated solutions, version 7.2.4) and the strain is calculated by the displacement of the speckle pattern. Tensile tests were performed on the sintered S, S-Cu and S-Al_2O_3 samples and their DIC measured strains are presented in **Video S1**, **S2** and **S3**, respectively. Five specimens for each sample type are tested.

Results and discussion

Steel scaffolds (S), steel scaffolds with copper support (S-Cu) and steel scaffolds with alumina support (S-Al_2O_3) are printed and thermally treated to investigate the influence of the support materials to the building structures. **Figure 2a** shows optical and SEM images of as-printed and sintered (thermally treated) S, S-Cu and S-Al_2O_3 scaffolds. The as-printed steel scaffolds supported by copper and alumina are as neat and orderly structured as the as-printed steel scaffold without support. The steel, copper and alumina particles are bound by the PLA binder to hold the structures, respectively. After the thermal treatment, the steel scaffolds retain their geometry, but exhibit some dimensional shrinkage. The SEM images of the sintered (thermally treated) scaffolds at different magnifications are presented in **Figure S3**. They have similar linear size reduction ranging from 10.7% to 11.2% (**Figure 2b**). Each type of steel scaffolds has a small size deviation of ≤1.3% (**Figure 2b**). The small deviation guarantees the reproducibility of this method in terms of dimensional accuracy of the fabricated structures. The steel particles of the S-Al_2O_3 scaffold are just as sintered as those in the S scaffold, but the S-Al_2O_3 scaffold has a rougher surface. The steel particles in S-Cu scaffold are sintered as well. In addition, the copper support melts and infiltrates into the sintered steel structure, leading to a smoother surface.

Figure 2c shows the single filament surface roughness (named as micro R_a) and the inter-filament surface roughness (termed as meso R_a) of the sintered steel scaffolds, and SEM images of the measured surfaces serving as an example of the micro and meso R_a. The profilometer probe traveling direction (measuring direction) is perpendicular to the filament longitudinal axis. The micro R_a of sintered S-Al_2O_3 (4.1μm) is greater than that of sintered S (2.5μm), while the micro R_a of sintered S-Cu (1.6μm) is smaller than that of sintered S. The meso R_as of sintered S and sintered S-Cu are similar (~5μm), which are smaller than that of sintered S-Al_2O_3 (13.9μm). The thermally treated alumina scaffold is so fragile that the shrinkage and surface roughness could not be measured. The shrinkage difference between the thermally treated ceramic particles and the sintered steel particles leads to a rougher surface. According to our observations, the support materials have little influence on the dimensional shrinkage of the steel scaffolds. The alumina support appears to increase the micro and meso surface roughness of the sintered steel structure by 1.6μm and 9μm, respectively.

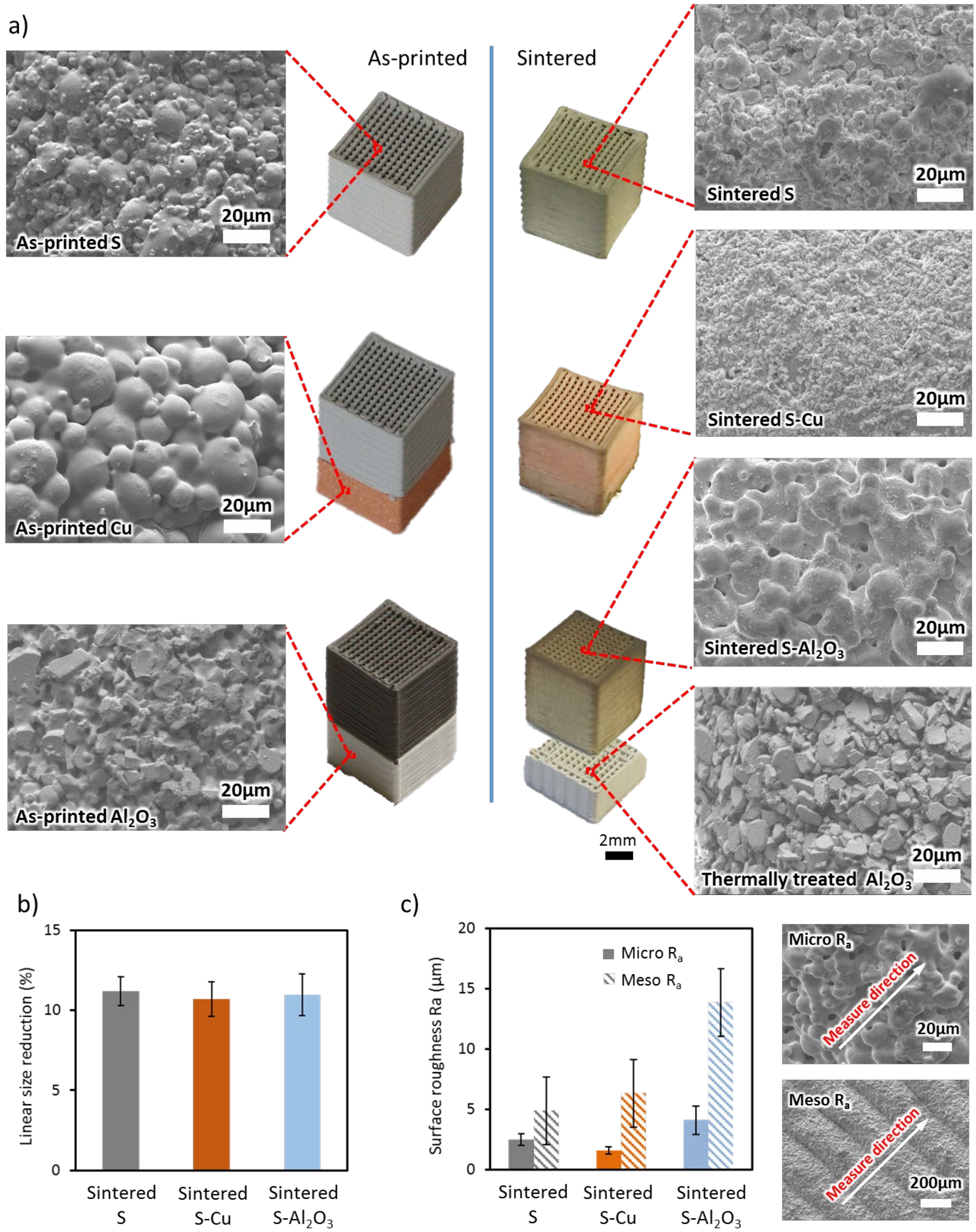

Figure 2. (a) Optical and SEM images of as-printed and sintered (thermal treated) scaffolds. (b) Linear size reduction of the sintered steel structures. (c) Single filament surface roughness (micro R_a) and inter-filament surface roughness (meso R_a) of the sintered steel structures, and SEM images of the measured surfaces serving as an example of the micro and meso R_a.

The influence of the support materials to the elemental composition and porosity of the building structures is studied through SEM and elemental analysis. **Figure 3a** shows SEM images and Energy-dispersive X-ray spectroscopy (EDS) elemental mappings of the cross sections of sintered S, sintered S-Cu, and sintered S-Al_2O_3 structures. The cross sections of the three types of sintered steel structures are characterized by the strong presence of iron. Copper is detected only in the sintered S-Cu structures as expected. The detection of copper is located in the regions between the iron rich zones. Aluminum and oxygen (i.e., the elements contained in the alumina support) are not detected in the sintered S-Al_2O_3 structures. Neither in the sintered S and sintered S-Cu structures. The elemental analysis result shows that: (i) the copper support infiltrates into the building structure and fills the majority of the pores in the sintered steel structure during the thermal treatment, and (ii) the alumina support is chemically stable during the thermal treatment and does not contaminate the steel structure. The volume fractions of the solid phases (iron for S and S-Al_2O_3, iron and copper for S-Cu) are similar in all three types of sintered steel structures at ~ 98% (**Figure 3b**). In the sintered S-Cu structure, the iron phase takes up about 87.2% and the copper phase accounts for around 10.4%. This value can be controlled by the volume ratio of the support and building structure, which will be studied in the future work. All the three types of sintered steel structures have similar and low porosity (~2%), and small pore size between 2 and 3 μm (Figure 3c-d). The supports do not have an obvious influence on the porosity and pore size to the building structure.

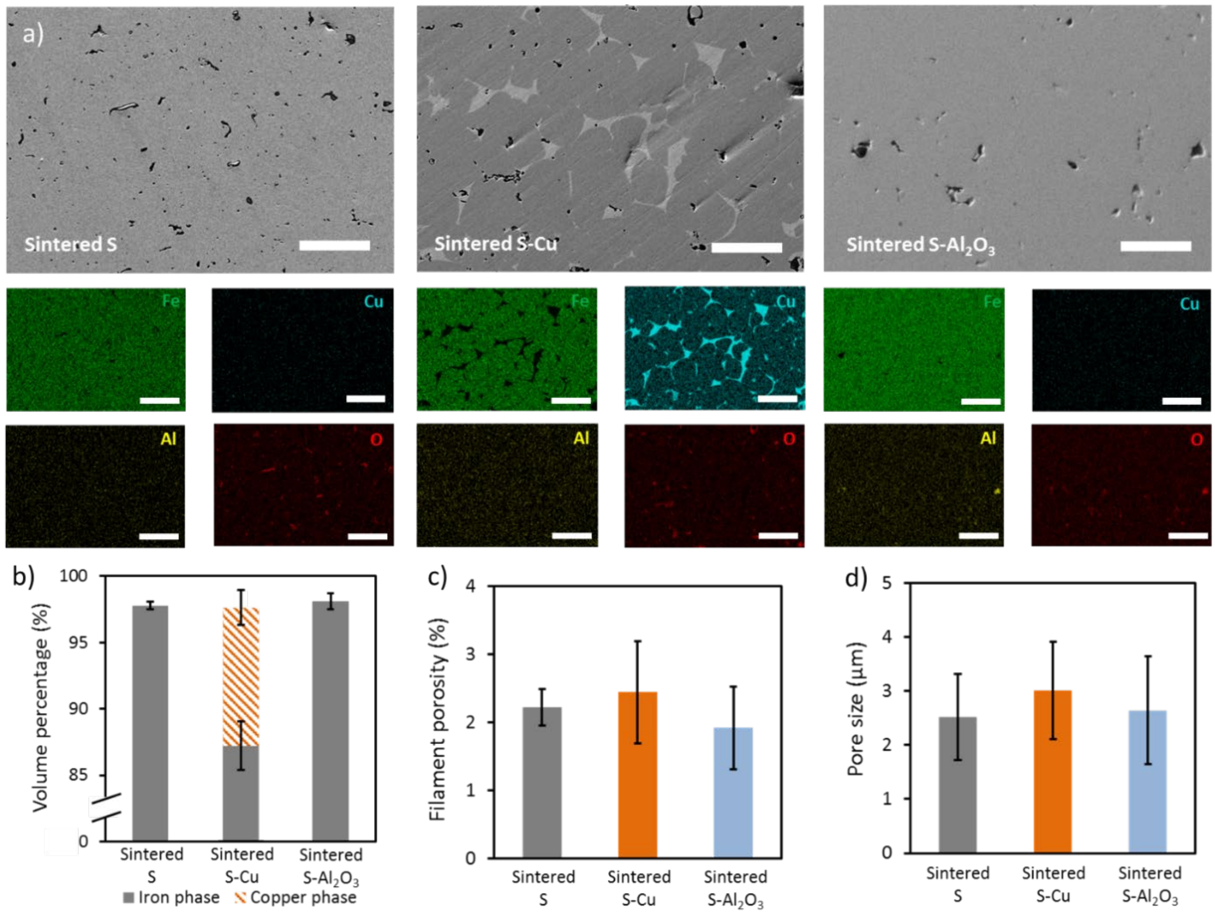

Figure 3. Elemental and porosity analysis of the sintered steel structures. (a) SEM images and EDS elemental mappings of the cross sections of sintered S, sintered S-Cu, and sintered S-Al_2O_3 structures. Scale bar = 50μm. (b) Volume percentage of iron and copper phase, (c) filament porosity, and (d) filament pore size of the various sintered steel structures.

Figure 4 shows the results for the electrical and tensile tests conducted on the sintered steel structures manufactured using different support materials.. **Figure 4a** presents typical tensile stress-strain curves and representative optical image of the sintered S, S-Cu and S-Al_2O_3 tensile bars in the inset. **Figure S4** presents the SEM images of the sintered S, S-Cu and S-Al_2O_3 fully dense tensile bars. Stereoscopic digital image correlation (DIC) technique is used to measure the strain in the tensile bars during the tensile tests (**Figure S5**). The measured tensile properties of the sintered steel structures are shown in **Figure 4b**. Sintered S-Cu exhibits higher Young's modulus E (174 ± 10 GPa), yield strength (YS) (284 ± 16 MPa) and ultimate tensile strength

(*UTS*) (521 ± 57 MPa) and elongation at failure (11.3% ± 3.6%) compared to those of sintered S (~30% - 45% superior). This increase in tensile properties is the result of copper infiltration of the sintered steel structure. Sintered S-Al_2O_3 has weaker tensile properties compared to the sintered S. The *E* (108 ± 6 GPa), the *YS* (165 ± 8 MPa) and the *UTS* (304 ± 18 MPa) of sintered S-Al_2O_3 are 15% - 21% less than those of sintered S. The elongation at failure (10.1% ± 1.4%) of sintered S-Al_2O_3 is similar to that of sintered S. We believe that the dimensional shrinkage difference between the steel structure and the alumina support might affect the sintering of the steel structure and lead to weaker tensile properties. **Figure 4c** shows the SEM images of the tensile fracture surfaces of the sintered steel tensile bars. More SEM images of the tensile fracture surfaces at different magnification are presented in **Figure S6**. The tensile fracture surface of the sintered S shows the shape and orientation of individual filaments at 45° relative to the tensile direction and orthogonal with the filaments from adjacent layers. Each individual filament is dense and the filaments from the same and the neighboring layers are fused together. The individual filament shape and orientation are recognizable but not very clear in the sintered S-Al_2O_3. The filaments in sintered S-Cu are completely fused together with the presence of copper, making a fully dense structure. The electrical conductivity of the sintered S-Al_2O_3 is $(6.9 \pm 3.4) \times 10^5$ S/m and the sintered S, $(7.4 \pm 0.4) \times 10^5$ S/m are similar (**Figure 4d**). The electrical conductivity of sintered S-Cu, $(27.9 \pm 4.2) \times 10^5$ S/m, is approximately four times higher than the value measure for the sintered S due to the presence of copper (**Figure 4d**). The properties of the sintered steel structures are summarized in **Table S1**. The overall electrical and mechanical properties of the sintered S-Cu are superior to those of the sintered S. Sintered S-Al_2O_3 has comparable electrical properties, but slightly weaker mechanical properties compared to the sintered S.

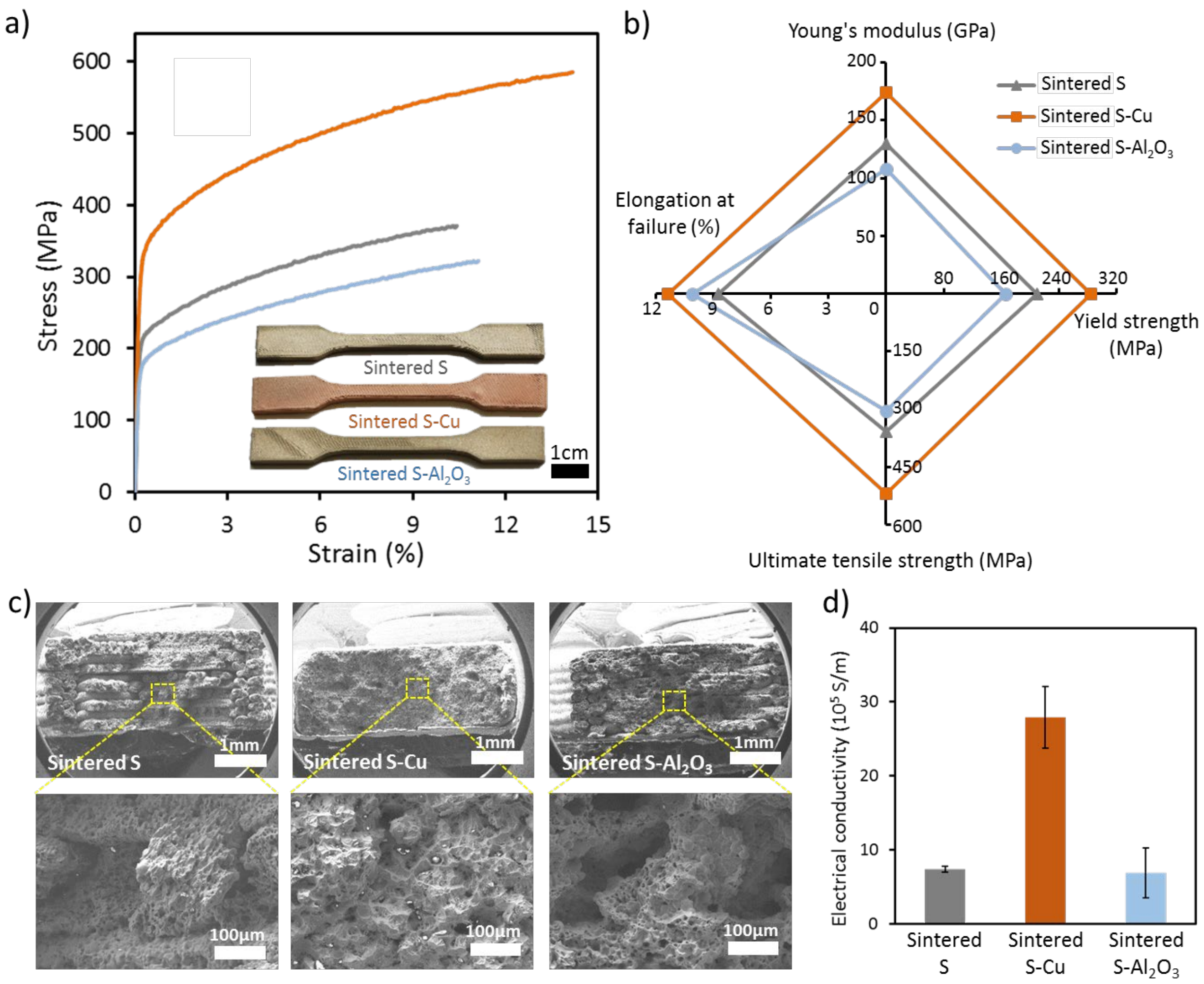

Figure 4. Electrical and mechanical characterizations of the sintered steel structures. (a) Typical tensile stress-strain curves of sintered steel structures and representative optical image of the different sintered steel tensile bars (inset). (b) Young's modulus, yield strength, ultimate tensile strength and elongation at failure of the sintered steel structures. (c) SEM images of the tensile fracture surfaces of the sintered steel structures. (d) Electrical conductivity of the sintered steel structures.

Conclusion

A multi-material direct ink writing method is developed to fabricate complex 3D metallic structures by printing removable supports using two different secondary materials. As a proof of concept, steel structures are fabricated through this method with the help of copper and alumina supports, respectively. The influence of the support materials on the steel structure is investigated. The supports lead to no significant difference to the building structures on the dimensional shrinkage, surface roughness and porosity of the building structure. The copper support brings a hybrid metallic composition to the steel structure and improves its electrical conductivity by four times and stiffness by 34%. Although the alumina supports lower the stiffness of the building structure by 17%, it brings no contamination to the steel structure. It is worth mentioning that the support materials are not only limited to copper or alumina. Any desired alloying metal with a lower melting point than the building material can be the metal support material, e.g., zinc and aluminum. Any ceramic material that is physically and chemically stable during the thermal treatment can be the ceramic support materials such as tungsten carbide. The proposed method broadens the geometry possibilities of metallic 3D structures that DIW can create. It provides the metal additive manufacturing of medical implants, sensors and batteries featuring complex geometries a readily accessible choice.

Supporting Information

SEM images, the strain distribution measured by DIC, a summary of the properties of the sintered steel structures, videos of the tensile test process with DIC measured strain showing on the samples.

Author Contributions

The manuscript was written through contributions of all authors. All authors have given approval to the final version of the manuscript.

Corresponding Author

(Daniel Therriault) Email: daniel.therriault@polymtl.ca

Conflict of Interest

The authors declare no conflict of interest.

Acknowledgements

The authors acknowledge the financial support from NSERC (Natural Sciences and Engineering Research Council of Canada, grant number: RGPIN 312568-2013) and Auto 21 of the Canadian Network of Centers of Excellence (NCE) program. The authors also acknowledge the scientific discussions from Olivier Sioui-Latulippe and Vincent Wuelfrath-Poirier on metallurgy science. A scholarship for Mr. Xu was also provided by the China scholarship Council (CSC) and the Fonds de recherche du Quebec - Nature et technologies (FRQNT).

References

1. Cheng, M., Jiang, Y., Yao, W., Yuan, Y., Deivanayagam, R., Foroozan, T., Huang, Z., Song, B., Rojaee, R., Shokuhfar, T., Pan, Y., Lu, J., Shahbazian-Yassar, R. Elevated-Temperature 3D Printing of Hybrid Solid-State Electrolyte for Li-Ion Batteries. *Adv. Mater.* **2018**, 30, 1800615.
2. Finsterbusch, M., Danner, T., Tsai, C.L., Uhlenbruck, S., Latz, A., Guillon, O. High Capacity Garnet-Based All-Solid-State Lithium Batteries: Fabrication and 3D-Microstructure Resolved Modeling. *ACS Appl. Mater. Interfaces* **2018**, 10, 22329–22339.
3. Elahinia, M., Moghaddam, N.S., Andani, M.T., Amerinatanzi, A., Bimber, B.A., Hamilton, R.F. Fabrication of NiTi through Additive Manufacturing: A Review. *Prog. Mater. Sci.* **2016**, 83, 630-663.
4. Amin Yavari, S., Loozen, L., Paganelli, F.L., Bakhshandeh, S., Lietaert, K., Groot, J.A., Fluit, A.C., Boel, C.H.E., Alblas, J., Vogely, H.C., Weinans, H. Antibacterial Behavior of Additively Manufactured Porous Titanium with Nanotubular Surfaces Releasing Silver Ions. *ACS Appl. Mater. Interfaces* **2016**, 8, 17080-17089.
5. Rim, Y.S., Bae, S.H., Chen, H., De Marco, N., Yang, Y. Recent Progress in Materials and Devices toward Printable and Flexible Sensors. *Adv. Mater.* **2016**, 28, 4415-4440.
6. Xu, L., Gutbrod, S.R., Bonifas, A.P., Su, Y., Sulkin, M.S., Lu, N., Chung, H.J., Jang, K.I., Liu, Z., Ying, M., Lu, C., Webb, R. C., Kim, J. S., Laughner, J. I., Cheng, H., Liu, Y., Ameen, A., Jeong, J. W., Kim, G. T., Huang, Y., Efimov, I. R., Rogers, J. A. 3D Multifunctional Integumentary Membranes for Spatiotemporal Cardiac Measurements and Stimulation across the Entire Epicardium. *Nat. Commun.* **2014**, 5, 4329.
7. Gu, D.D., Meiners, W., Wissenbach, K. Poprawe, R. Laser Additive Manufacturing of Metallic Components: Materials, Processes and Mechanisms. *Int. Mater. Rev.* **2012**, 57, 133-164.

8. Herzog, D., Seyda, V., Wycisk, E., Emmelmann, C. Additive Manufacturing of Metals. *Acta Mater.* **2016**, 117, 371-392.
9. Martin, J.H., Yahata, B.D., Hundley, J.M., Mayer, J.A., Schaedler, T.A., Pollock, T.M. 3D Printing of High-strength Aluminium Alloys. *Nature* **2017**, 549, 365.
10. Gong, H., Rafi, K., Gu, H., Ram, G.J., Starr, T., Stucker, B. Influence of Defects on Mechanical Properties of Ti–6Al–4 V Components Produced by Selective Laser Melting and Electron Beam Melting. *Mater. Des.* **2015**, 86, 545-554.
11. Olakanmi, E.O.T., Cochrane, R.F., Dalgarno, K.W. A Review on Selective Laser Sintering/Melting (SLS/SLM) of Aluminium Alloy Powders: Processing, Microstructure, and Properties. *Prog. Mater. Sci.* **2015**, 74, 401-477.
12. Chou, R., Milligan, J., Paliwal, M., Brochu, M. Additive manufacturing of Al-12Si Alloy via Pulsed Selective Laser Melting. *JOM* **2015**, 67, 590-596.
13. Skylar-Scott, M.A., Gunasekaran, S. and Lewis, J.A., Laser-assisted Direct Ink Writing of Planar and 3D Metal Architectures. *Proc. Natl. Acad. Sci. U. S. A.* **2016**, 113, 6137-6142.
14. Wang, X., Guo, Q., Cai, X., Zhou, S., Kobe, B. and Yang, J., Initiator-integrated 3D Printing Enables the Formation of Complex Metallic Architectures. *ACS Appl. Mater. Interfaces* **2013**, 6, 2583-2587.
15. Lewis, J. A. Direct Ink Writing of 3D Functional Materials. *Adv. Funct. Mater.* **2006**, 16, 2193-2204.
16. Therriault, D., White, S.R., Lewis, J.A. Chaotic Mixing in Three-dimensional Microvascular Networks Fabricated by Direct-write Assembly. *Nat. Mater.* **2003**, 2, 265.
17. Ahn, B.Y., Shoji, D., Hansen, C.J., Hong, E., Dunand, D.C., Lewis, J.A. Printed Origami Structures. *Adv. Mater.* **2010**, 22, 2251-2254.

18. Jakus, A.E., Taylor, S.L., Geisendorfer, N.R., Dunand, D.C., Shah, R.N. Metallic Architectures from 3D-printed Powder-based Liquid Inks. *Adv. Funct. Mater.* **2015**, 25, 6985-6995.

19. Xu, C., Bouchemit, A., L'Espérance, G., Lebel, L.L., Therriault, D. Solvent-cast based Metal 3D Printing and Secondary Metallic Infiltration. *J. Mater. Chem. C* **2017**, 5, 10448-10455.

20. Xu, C., Wu, Q., L'Espérance, G., Lebel, L.L., Therriault, D. Environment-friendly and Reusable Ink for 3D Printing of Metallic Structures. *Mater. Des.* **2018**, 160, 262-269.

21. Ziemian, C.W., Crawn III, P.M. Computer Aided Decision Support for Fused Deposition Modeling. *Rapid Prototyp J* **2001**, 7, 138-147.

22. Waheed, S., Cabot, J.M., Macdonald, N.P., Lewis, T., Guijt, R.M., Paull, B., Breadmore, M.C. 3D Printed Microfluidic Devices: Enablers and Barriers. *Lab Chip* **2016**, 16, 1993-2013.

23. Peckner, D., Bernstein, I. M. *Handbook of Stainless Steels*; McGraw-Hill Book Company, New York, 1997.

24. Davis, J. R. *Copper and Copper Alloys*; ASM international, 2001.

25. Pradyot, P. *Handbook of Inorganic Chemicals*; McGraw-Hill, New York, 2003.

Table of Contents

A multi-material direct ink writing (DIW) method is developed to fabricate complex three-dimensional (3D) steel structures by creating a removable support printed from a lower melting temperature metal (i.e., copper) or a ceramic (i.e., alumina). The lower melting temperature metal completely infiltrates the porous steel structures for a hybrid configuration, while the ceramic offers a brittle support that can be easily removed.

Keyword: additive manufacturing, direct ink writing, complex 3D metallic structures, removable support, multi-material

Authors: *Chao Xu, Bronagh Quinn, Gilles L'Espérance, Louis Laberge Lebel, Daniel Therriault**

Title: Multi-material direct ink writing (DIW) for complex 3D metallic structures with removable supports